LARGE EDDY SIMULATION OF A SUPERSONIC CAVITY FLOW WITH AN UNSTRUCTURED GRID FLOW SOLVER

BRIAN R. SMITH
Lockheed Martin Aeronautics Company
Fort Worth, Texas 76101

Abstract

Large Eddy Simulation methods were implemented in a hexahedral based unstructured grid flow solver and tested for the analysis of transonic flow over an open cavity. This approach was developed for efficient application of Computational Fluid Dynamics methods to the highly unsteady flows in a geometrically complex weapons bay. A compressible sub grid scale model was implemented. The compressible flow solver uses an upwind flux difference splitting scheme. A Mach 1.2 flow over an open cavity was simulated. Comparisons of computed and experimental spectra of the sound pressure level at several locations in the cavity are presented. Good agreements between the simulations and test were obtained.

1. Introduction

Weapons bay flowfields present significant design challenges for tactical aircraft. Unsteady resonant phenomena in an open bay can result in unsteady pressure levels above 170 dB. The aircraft structure, weapons bay doors and internally carried stores can be damaged by loads of this magnitude. Accurate prediction of these loads is important for the structural design of the aircraft, determination of suitability of stores for the weapons bay environment, and assessment of devices used for control and suppression of acoustic loads. Computational methods for predicting these loads will be useful in reducing the significant testing cost and design cycle time required for bay design and weapons integration.

A typical weapons bay geometry is highly complex and includes bulkheads, irregularly shaped doors, loaded stores with fins, and launchers. Generation of a structured mesh for this type of complex geometry is impractical because of the large number of man hours required. For simulation, unsteady Reynolds averaged Navier-Stokes methods have proven to be excessively diffusive for cavity simulation. Several studies have demonstrated the use of structured grid methods with Large Eddy Simulation (LES) for simple cavity flows.[1] In this work, LES methods implemented in the Lockheed Martin Aeronautics Splitflow unstructured grid solver are applied to a simple cavity flow to assess the accuracy of the methodology.

2. Numerical Methods

The Splitflow code includes two grid generation approaches, both of which are used in this work. The LES method implemented in Splitflow includes filter length smoothing required by the unique nature of Splitflow grids. The strong, moving shockwaves generated in a cavity flow are the motivation for the use of an upwind flow solver for the cavity simulations. Background information on Splitflow is available in the paper by Domel and Karman.[2]

2.1 Grid Generation Two grid generation options are available in Splitflow. The first, "cut grid" method, is a tree based splitting method for Cartesian cells. Cells aligned with the Cartesian axes are refined by splitting into two, four or eight cells. A triangulated surface mesh is used to define solid boundaries. Where Cartesian cells are cut by the triangulated surfaces, irregularly shaped cells result. Cells can be refined to flowfield gradients and structures in the course of a run by subdividing and recombining cells. The refinement process does not require re-generation of the entire mesh, and is therefore highly efficient. In the second, "body conforming" method, cells cut by boundary surfaces are deleted, and new body conforming cells are created by extrapolating from the inner cell faces to the surface. The resulting grid is then smoothed to improve grid quality. In this approach, the resulting grid is not aligned with the coordinate axes, and grid generation requires more computer time to complete than in the "cut grid" approach.

Both approaches are highly automated and require very few man hours to develop computational grids for complex configurations. The "cut grid" method is best suited to applications where high fidelity boundary layer resolution is not required, or where walls are aligned with Cartesian axes. The "boundary conforming" approach is best suited to problems requiring high fidelity simulation of turbulent boundary layers.

Because of the cell splitting approach, both types of Splitflow grids are extremely well suited to LES. Near no slip walls, the computational mesh can be refined in normal, lateral and streamwise directions, while coarser grids can be used in all three directions away from the wall.

2.2 LES Methods A compressible form of the Smagorinsky model was used.[3] The sub grid scale stresses are represented by a Favre mass averaged Bousinesq approximation using the mean velocities. The eddy viscosity is

$$\mu_t = \rho\ l^2 |S|, \text{ where } |S| = \sqrt{2 S_{ij} S_{ij}}$$

and $S_{ij} = \frac{1}{2}(\partial U_i/\partial x_j + \partial U_j/\partial x_i)$ is the strain tensor. The mixing length, l, is the product of the Smagorinsky constant, C_s, and the filter length, Δ. The constant C_s

is set to 0.1 for this study. Initially the filter length is set $\Delta = (\text{cell volume})^{1/3}$. However, unlike a structured grid, neighboring Splitflow cells can vary in volume by a factor of 8, resulting in a doubling of the filter length across a cell face. This is inconsistent with sub grid scale filtering assumptions. To alleviate this problem, the filter length at each cell is smoothed in multiple passes through a smoothing routine that sets the filter length equal to the average of the maximum of the filter length for the current cell and all of its immediate neighbors,

$$\Delta_c^{p+1} = \frac{1}{N}\sum_{n=1}^{N} \max(\Delta_c^p, \Delta_n^p)$$

where N is the number of neighboring cells, and p is the sweep index. This approach provides a smoother variation in the filter length through the flowfield. Regions of locally fine mesh effectively have a larger value of eddy viscosity. As a result, the numerical accuracy of the flow solver is improved by reduction in truncation error, but the level of the sub grid scale stresses in regions of locally fine mesh is higher than it would be if the mesh were more uniformly fine.

2.3 Flow Solver Methods The flow domain is segmented into multiple subdomains and solved in parallel using PVM. The convective terms are evaluated using a third order accurate, finite volume upwind scheme. The primitive variables, (ρ, u, v, w, T) are extrapolated to the left and right sides of each cell face using the cell center gradients of the primitive variables on each side of the cell face. The resulting left and right states are the basis for the upwind diffusion term. This approach is formally third order accurate where cells are evenly spaced, and second order accurate where cell division creates local variations is cell size. In regions of the flow field with strong shock waves, a flux limiter is employed.

Because the cavity application has strong shocks, a compressible solution algorithm including the Roe upwind flux difference split scheme is employed.[4] This scheme is considerably less diffusive in low speed and wall boundary layer regions than flux vector split algorithms. Nevertheless, the scheme tends to damp unsteady flow structures in wall boundary layers, particularly when the local flow velocity is not aligned with the grid direction. The diffusion term was reduced by multiplying it by a function of the ratio of the contravarient velocity to the local velocity magnitude. This approach significantly reduces the damping of unsteady structures while providing sufficient upwind influence for numerical stability.

The solution is advanced in time using a pointwise block implicit algorithm. In order to obtain second order accuracy in time, multiple sub-iterations are employed to converge the solution at each time step. This approach allows local CFL numbers significantly larger than one to be used. For compressible flow

simulations with fine grid spacing normal to the wall, the acoustic wave speed can severely limit the allowable time step.

3. Cavity Flow Application

A cavity flow from the Weapons Internal Carriage and Stores test was used to evaluate the code's accuracy.[5] The geometry tested was a simple rectangular cavity in a model with a sharp leading edge. The model has a 15 inch long, 16.5 inch wide flat plate in front of the cavity. The LxWxD of the cavity is 18"x4"x4". The Mach number for the demonstration case is 1.2, the Reynolds number per foot of the flow is 1.0×10^6. The diagram of the cavity in Figure 1 includes relevant sensor locations.

3.1 Simulation Approach To reduce the computational requirements, a turbulent channel flow was used to generate a turbulent boundary layer for the inflow boundary condition for the cavity flow simulation. The channel flow domain is two inches long, one inch wide and its height is 0.56 inches, twice the incoming boundary layer thickness of the cavity flow. The Reynolds number for the channel based on half the channel height is 19,000. Periodic boundary conditions are applied in the lateral and streamwise directions. Flow pressure, momentum and total enthalpy are adjusted between the inflow and outflow periodic boundaries to account for compressibility effects. A cut grid mesh containing 138,000 cells was generated. Figure 2 shows a cross section view of the channel grid. The near wall spacing was $\Delta z^+ = 1.7$, $\Delta y^+ = 29$, $\Delta x^+ = 58$. The channel outflow solution was repeated across the lateral "y" direction to span the cavity inflow. The channel and cavity solutions were run simultaneously, and information was passed at each iteration from the channel to the cavity flow solution.

The cavity grid was generated using the body conforming approach. The grid contains 614,000 cells. The grid is most highly resolved in the shear layer near the leading edge of the cavity. Figure 3 shows a centerline view of the cavity grid.

The solutions were performed using a time step of 5×10^{-7} second. Over 60,000 iterations were completed. Figure 4 shows instantaneous velocity contours along the centerline of the cavity. Figure 5 shows instantaneous velocity contours 2, 10 and 16 inches downstream of the leading edge of the cavity. Vortical structures at the edge of the cavity near the trailing edge are clearly visible. The shear layer disturbances are much smaller near the cavity leading edge.

Sound pressure level spectra from test and simulation at four locations in the cavity are shown in Figure 6. The simulation clearly captures most of the resonant tones in the cavity. In addition, the levels are predicted with reasonable accuracy.

The significant variations in the SPL between the front and back wall of the cavity are also predicted well.

Acknowledgements This work was funded by AFOSR under the "Large Eddy Simulation for the Analysis of Weapons Bay Flows" program, Contract No. F49620-99-C-0020. The author would like to thank Dr. Leonidas Sakell and Dr. Robert Herklotz for their support.

References

1. Smith, B. R., Jordan, J. K., Bender, E. E., Rizk, S. N. and Shaw, L. L., "Computational Simulation of Active Control of Cavity Acoustics," AIAA Paper 2000-1927, Lahaina, HI, June, 2000.

2. Domel, N. D. and Karman, S. L. "Splitflow: Progress in 3D CFD with Cartesian Omni-tree Grids for Complex Geometries,", AIAA Paper 2000-1006, Reno, NV, January, 2000.

3. Smagorinsky, J., "General Circulation Experiments with the Primitive Equations," Mon. Weather Rev., (1963), Vol. 91. pp. 99-164.

4. Roe, P. L., "Characteristic-Based Schemes for the Euler Equations," *Annual Review of Fluid Mechanics*, Vol. 18, 1986, pp. 337-365.

5. Dix, R. E. and Dobson, T. W. Jr., "Database for Internal Store Carriage and Jettison," Final Report, AEDC-TR-90-23.

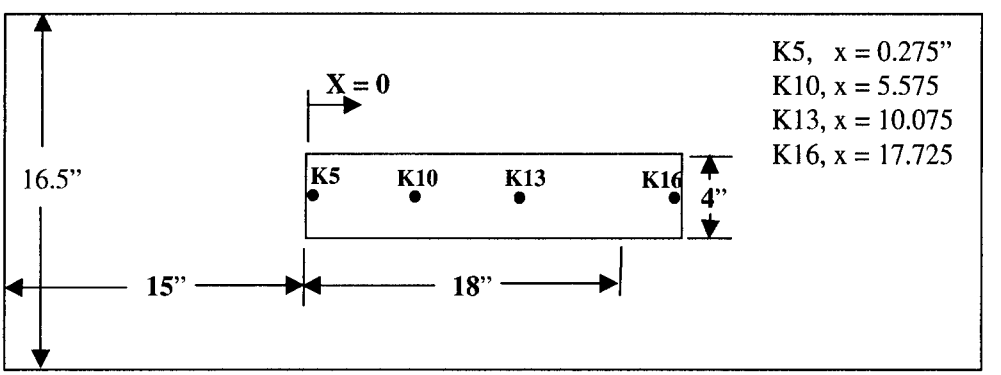

Figure 1 Diagram of cavity geometry including pressure sensor locations

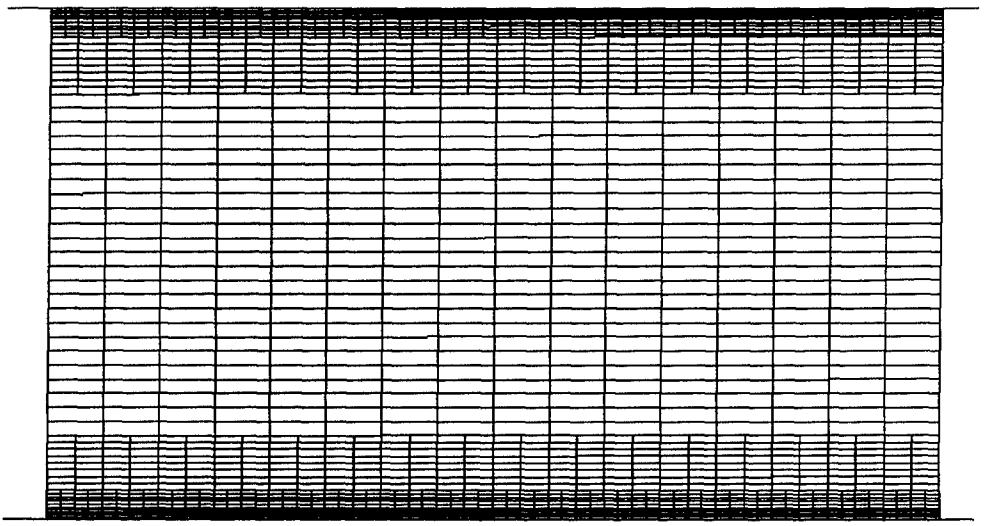

Figure 2 Cross section view of channel grid

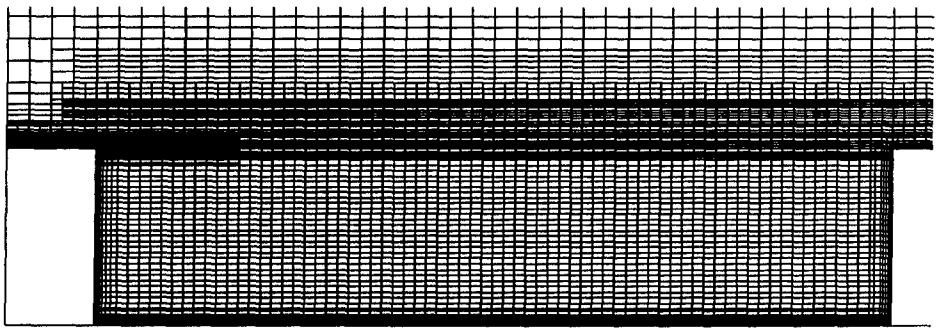

Figure 3 Centerline view of cavity grid

Figure 4 Contours of instantaneous stream wise velocity on cavity centerline.

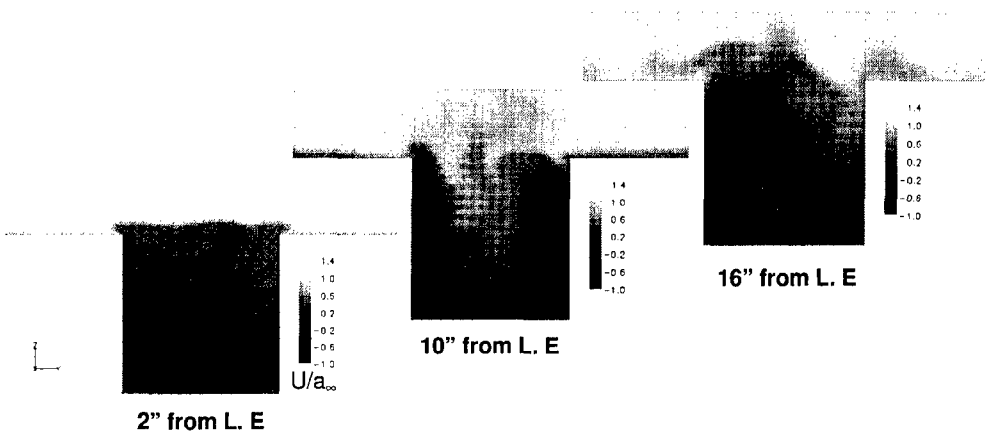

Figure 5 Contours of instantaneous stream wise velocity 2", 10" and 16" from cavity leading edge.

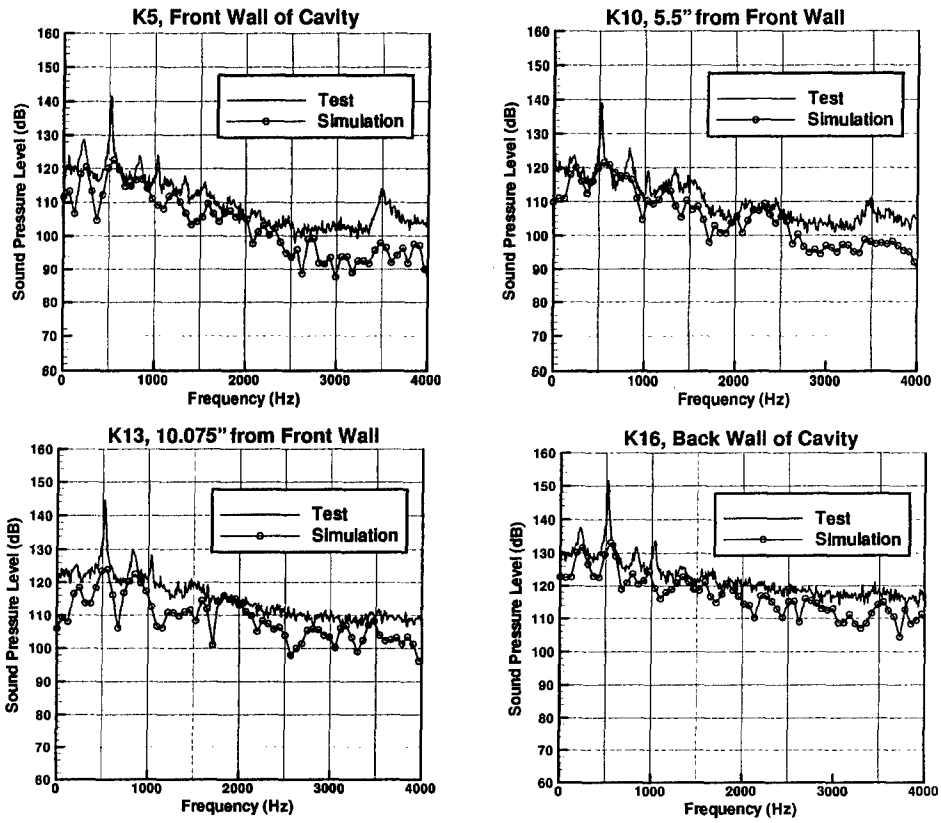

Figure 6 Test and simulation spectra of sound pressure level at pressure sensor locations.